High performance and cost-effective hybrid steel/CFRP joints using bi-adhesive technique for the repair of metallic infrastructures

Mohabeddine, Anis; Malik, Ghassan; Correia, José; De Jesus, Abílio; Fantuzzi, Nicholas; Miguel Castro, José

DOI
10.1016/j.compstruct.2023.117284

Publication date
2023

Document Version
Final published version

Published in
Composite Structures

Composite Structures 321 (2023) 117284

Contents lists available at ScienceDirect

Composite Structures

journal homepage: www.elsevier.com/locate/compstruct

High performance and cost-effective hybrid steel/CFRP joints using bi-adhesive technique for the repair of metallic infrastructures

Anis Mohabeddine [1,*], Ghassan Malik [2], José Correia [3], Abílio De Jesus [4], Nicholas Fantuzzi [5], José Miguel Castro [6]

[1] Faculty of Civil Engineering and Geosciences, Delft University of Technology, the Netherlands
[2] DICAM – Department, School of Engineering and Architecture, University of Bologna, Italy
[3] INEGI & CONSTRUCT, Faculty of Engineering, University of Porto, 4200-465 Porto, Portugal
[4] Faculty of Engineering, University of Porto, 4200-465 Porto, Portugal
[5] DICAM – Department, School of Engineering and Architecture, University of Bologna, Italy
[6] CONSTRUCT, Faculty of Engineering, University of Porto, 4200-465 Porto, Portugal

ARTICLE INFO

Keywords:
CFRP
Steel
Adhesive bonding
Strengthening
Metallic structures

ABSTRACT

The use of the brittle adhesives commonly adopted in construction industry do not provide the best performance for steel structures. CFRP/Steel joint bonded with extremely tough adhesive achieve much higher strength and ductility. However, tough adhesives are not developed for the construction industry and their cost may question the feasibility of this repair solution. This paper presents a new high performance and cost-effective hybrid bi-adhesive CFRP/Steel joint by using an extremely tough adhesive in critical location and the brittle adhesive in the remaining areas of the adhesive layer. The role of the tough adhesive in the proposed joint is fundamentally different from previous bi-adhesive joint proposed in the literature as it contributes mainly in shear. Experimental testing and finite element analysis are conducted. The Digital image correlation (DIC) is used to measure the strain field on the CFRP. The results revealed that the proposed CFRP/Steel hybrid joint achieve higher strength than the joints with brittle adhesive. The use of the tough adhesive in the bi-adhesive joint reduces the concentration of shear stresses significantly. As little quantities of the tough adhesive are required to manufacture the proposed bi-adhesive joint, it deemed to be as cost-effective.

1. Introduction

A large number of metallic structures are facing aging problems such as fatigue and corrosion that require a particular attention [1–5]. The replacement of all old structures is economically unfeasible. Therefore, the development of effective repair solutions is of paramount importance.

The application of bonded CFRP is a repair technique with a great potential to strengthen metallic structures and is gaining lot of interest from the industry. However, it is still at its early stages of application compared to mechanical engineering sub-industries. In the last two decades, several research studies focused on understanding the behaviour of CFRP/Steel adhesive joints [6–14] as the performance of the adhesive layer is the most critical part to obtain a successful application. Several influencing parameters were investigated such as: the surface preparation of the adherends [7,11,12], the stiffness of the CFRP [11], mechanical properties of the adhesive [7,16,17], thickness of the adhesive layer [7,18], and the bond length [19–21]. However, most of the previous research studies used brittle adhesives since cohesive failure mode can be easily achieved which facilitate the development of design procedures [7,8,22]. The brittle adhesives used in the construction industry bond well with metallic substrates however they were initially developed for concrete structures [25] and do not provide the best performance for metallic structures. The choice of the adhesive type has a significant influence on the performance of the steel/CFRP adhesive joints [23]. Recently developed tough adhesives with high strength and ductility are more appropriate for bonding metallic substrates [24]. Very recently, SIKA® [25] developed a moderately tough adhesive (i.e. SIKADUR-370) for the repair of steel bridges affirming that the highly brittle 2C-epoxy adhesives (such as SIKADUR-30 ubiquity used in

* Corresponding author.
E-mail addresses: a.i.mohabeddine@tudelft.nl (A. Mohabeddine), ghassanabdalla.malik@studio.unibo.it (G. Malik), jacorreia@fe.up.pt (J. Correia), ajesus@fe.up.pt (A. De Jesus), nicholas.fantuzzi@unibo.it (N. Fantuzzi), jmcastro@fe.up.pt (J. Miguel Castro).

https://doi.org/10.1016/j.compstruct.2023.117284
Received 8 January 2023; Received in revised form 5 May 2023; Accepted 17 June 2023
Available online 19 June 2023

Table 1
Average adhesives basic mechanical properties (this data was also published in [23]).

Adhesive	E (MPa)	Max stress (MPa)	Max Deformation (%)	Toughness (Jmm^{-3})
Sikadur 30	12,915	35.03	0.28	0.058
S&P HP220	7600	33.16	0.54	0.108
AW4858/ HW4858	1350	34.9	13.6	3.9

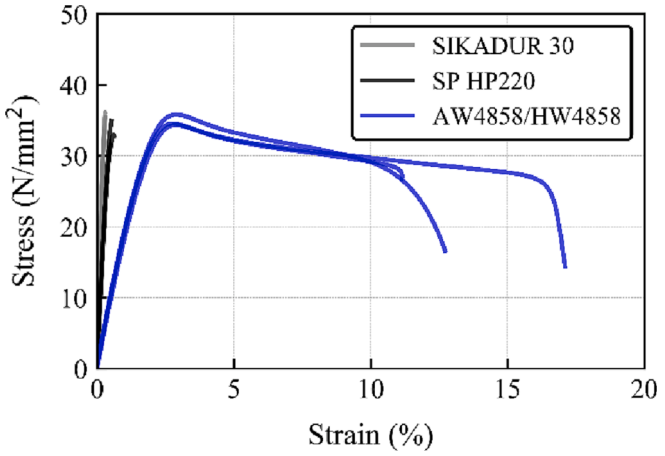

Fig. 1. Coupon test stress–strain curves (this data was also published in [23]).

Table 2
Basic mechanical and geometrical properties of the CFRP provided by the manufacturer [45].

Type	E (GPa)	Ultimate stress (MPa)	Elongation at break (%)	Thickness (mm)	Width (mm)
C-Laminate S&P HM 200/ 2000	205	2800	1.3%	1.4	50

research related to CFRP/Steel joints) are more suitable for concrete and other cementitious systems but for more ductile substrates such as steel toughened ductile adhesives should be used.

Nowadays, extremely tough adhesives can be found in the market. This type of adhesive provide very high performance suitable for metallic bridge repairs [23], however, they can be significantly more expensive than brittle adhesives used in the construction industry. In civil engineering structures, large amount of adhesive is required due to the size of the structural elements. The use of tough adhesives might be economically unfeasible. Therefore, the development of more economical solutions while maintaining the same level of performance of tough adhesives joints needs to be developed.

Several strengthening techniques of adhesive joints have been adopted in the literature, among them are: tapering the overlap and/or using large fillets of adhesive [26–30], stepped notches [31], reinforcement of the adhesive layer with metallic or organic fibres [32,33], and mixed adhesive joints [34]. Mixed adhesive joint or also called hybrid bi-adhesive joints have been firstly recognized by Hart-smith [35] for low and high temperature applications to extend the temperature range of the adhesive joint. Other researchers investigated bi-adhesive joints to improve the joint strength [34,36–40]. This technique consists of using a stiff and strong adhesive in the middle of the overlap and a very flexible and ductile adhesive at the ends of the overlap to relieve the high peeling stress at the ends and promotes a more uniform strain distribution. Past experimental results [34,37–40] revealed that some bi-adhesive joints can achieve higher strength than brittle adhesive alone. However, most the existing studies were developed for the aeronautical or automotive industry where the joint geometry, the overlap length, the adhesive type, and adherends are not representative to civil engineering metallic structures.

In this paper, a new high-performance hybrid bi-adhesive joint is proposed using mainly a brittle adhesive commonly used in the construction industry (due to its lower cost) and little amount of extremely tough adhesive applied at critical locations. The configuration as well as the behaviour differ significantly from previously proposed bi-adhesive joints. As in this case: a different type of adhesive is applied (i.e. tough adhesive that combine high strength and ductility instead of very ductile adhesive and low strength [39]), and a different location where to place the tough adhesive is adopted. The tough adhesive is placed in a way to resist shear stresses significantly instead of only peeling. Experimental

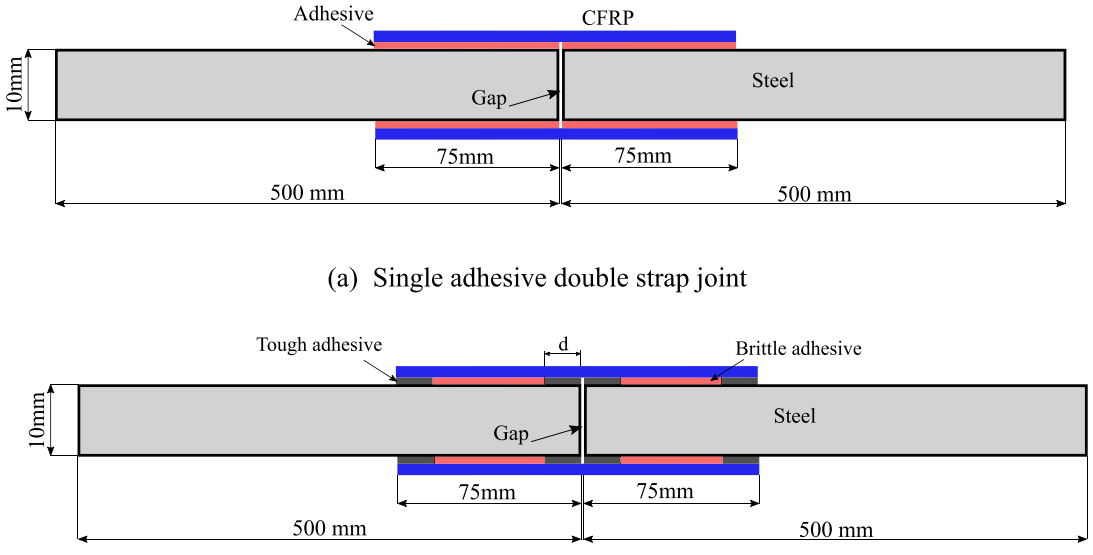

Fig. 2. Schematic view of a double strap joint (Adhesive thickness = 1*mm* and CFRP Thickness 1.4*mm*).

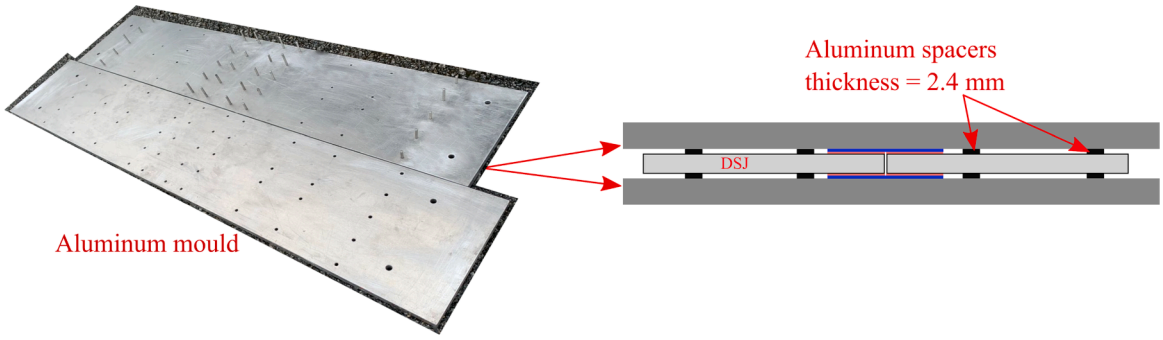

Fig. 3. Aluminium mould for the fabrication of DSJ specimens.

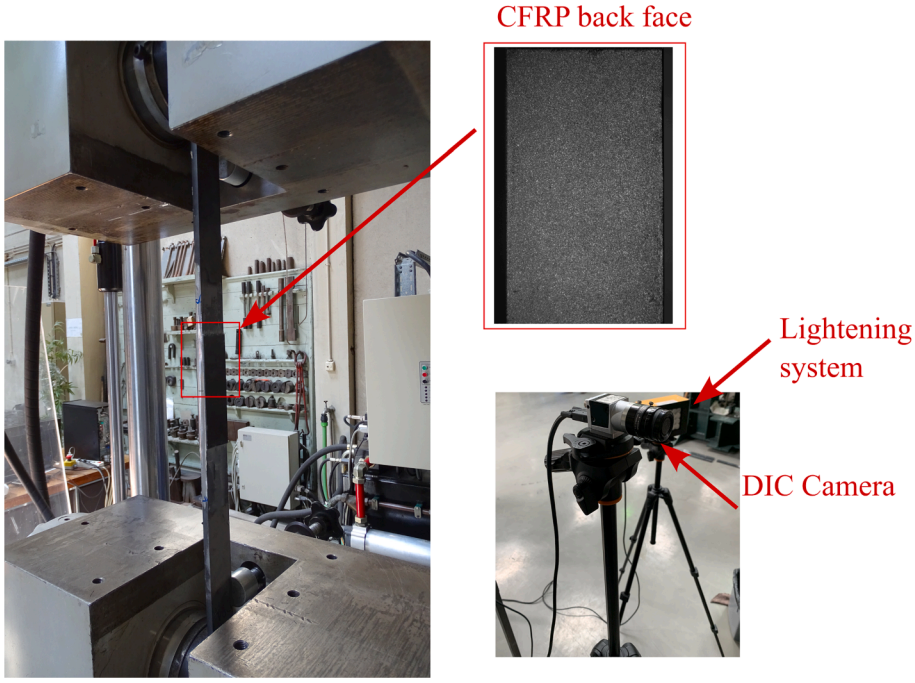

Fig. 4. Experimental set up.

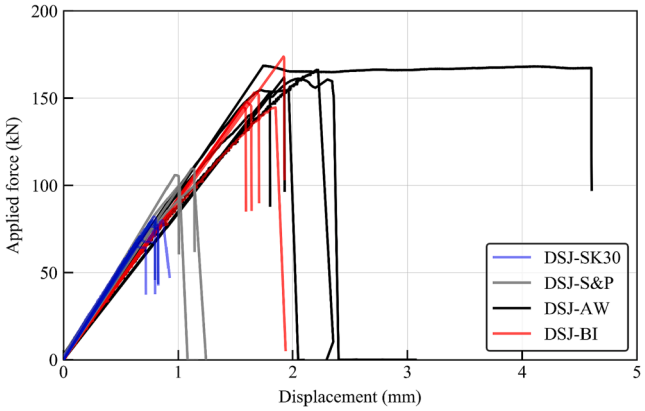

Fig. 5. DSJ specimens load displacement curves (Except DSJ-BI, the data was also published in [23]).

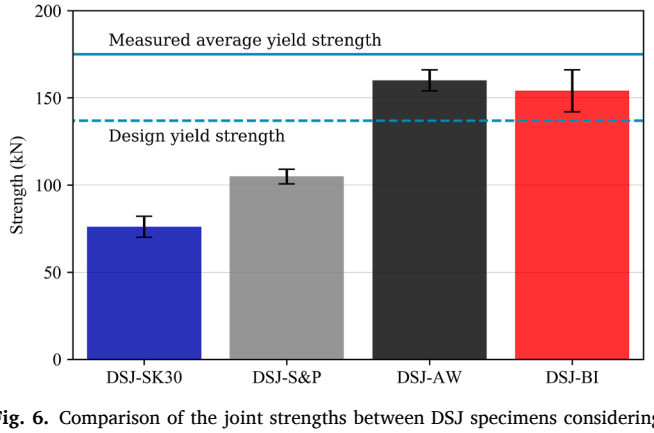

Fig. 6. Comparison of the joint strengths between DSJ specimens considering the design yield strength and measured average yield strength as reference.

testing of double strap joint (DSJ) is conducted to compare joints with brittle adhesives, an extremely tough adhesive alone, and bi-adhesive. The DIC is used to measure the strain fields at the back face of the CFRP due to the possibility of measuring the variation of deformation levels along the width and length which makes it particularly useful to detect defects and locations of stress concentrations which cannot be obtained using strain gauges as adopted in previous studies. A finite element model validated with experimental data is developed in ABAQUS. Based on the experimental and numerical results a comprehensive

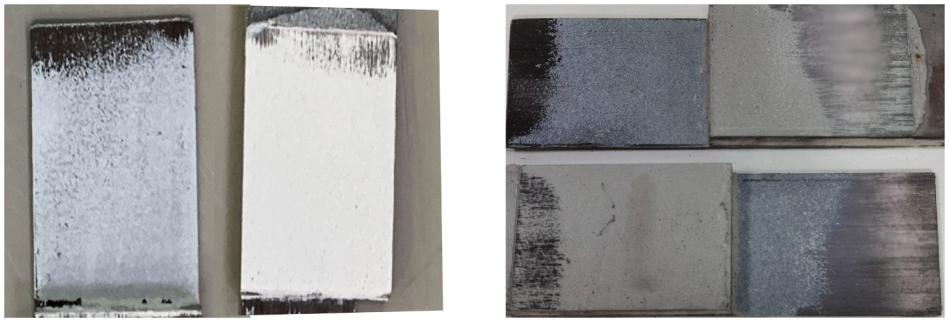

(a) DSJ-SK30

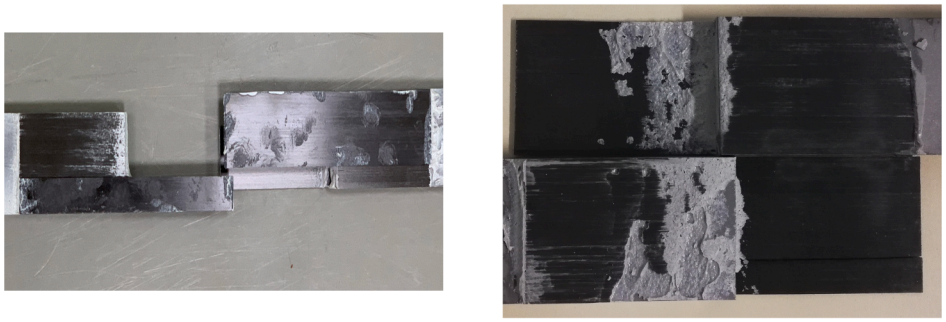

(b) DSJ-S&P

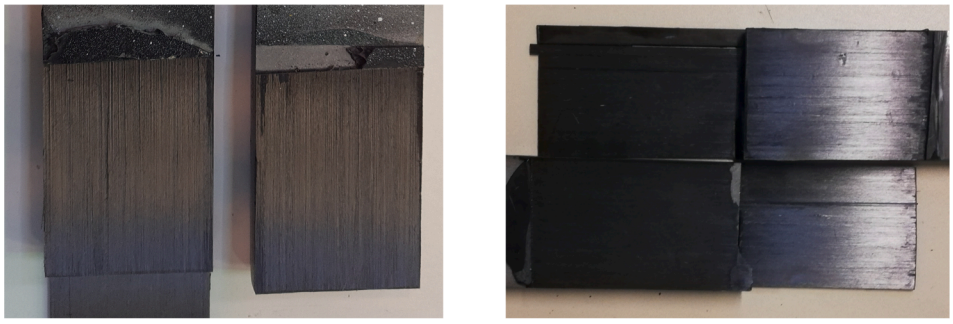

(c) DSJ-AW

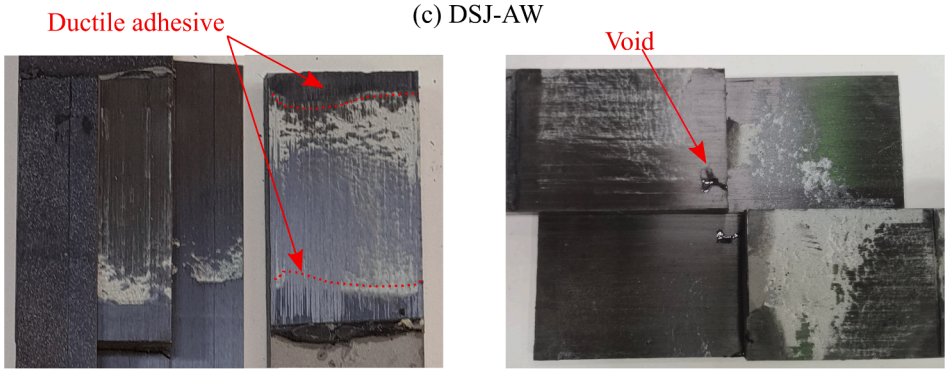

(d) DSJ-BI

Fig. 7. Typical failure mode for DSJ specimens: (a) DSJ-SK30, (b) DSJ-AW, (c) DSJ-S&P, and (d) DSJ-BI.

discussion on the behaviour, failure modes, and stress distribution is provided.

2. Experimental program

2.1. Materials

Three different adhesives have been used to bond the CFRP and the steel plates, which consist of:

- **Sikadur 30 (SK-30):** two components epoxy-based linear brittle adhesive used in the construction industry and the most common adhesive used research studies related to steel/CFRP joints. For more information see the manufacturer datasheet [41].
- **S&P HP220 (S&P):** two components epoxy-based linear rigid adhesive commonly used in the construction industry. For more information see the manufacturer datasheet [42].
- **Araldite AW4858/HW4858 (AW):** two component epoxy-based ductile adhesive developed for different mechanical engineering industries suitable for bonding a wide variety of metals, and

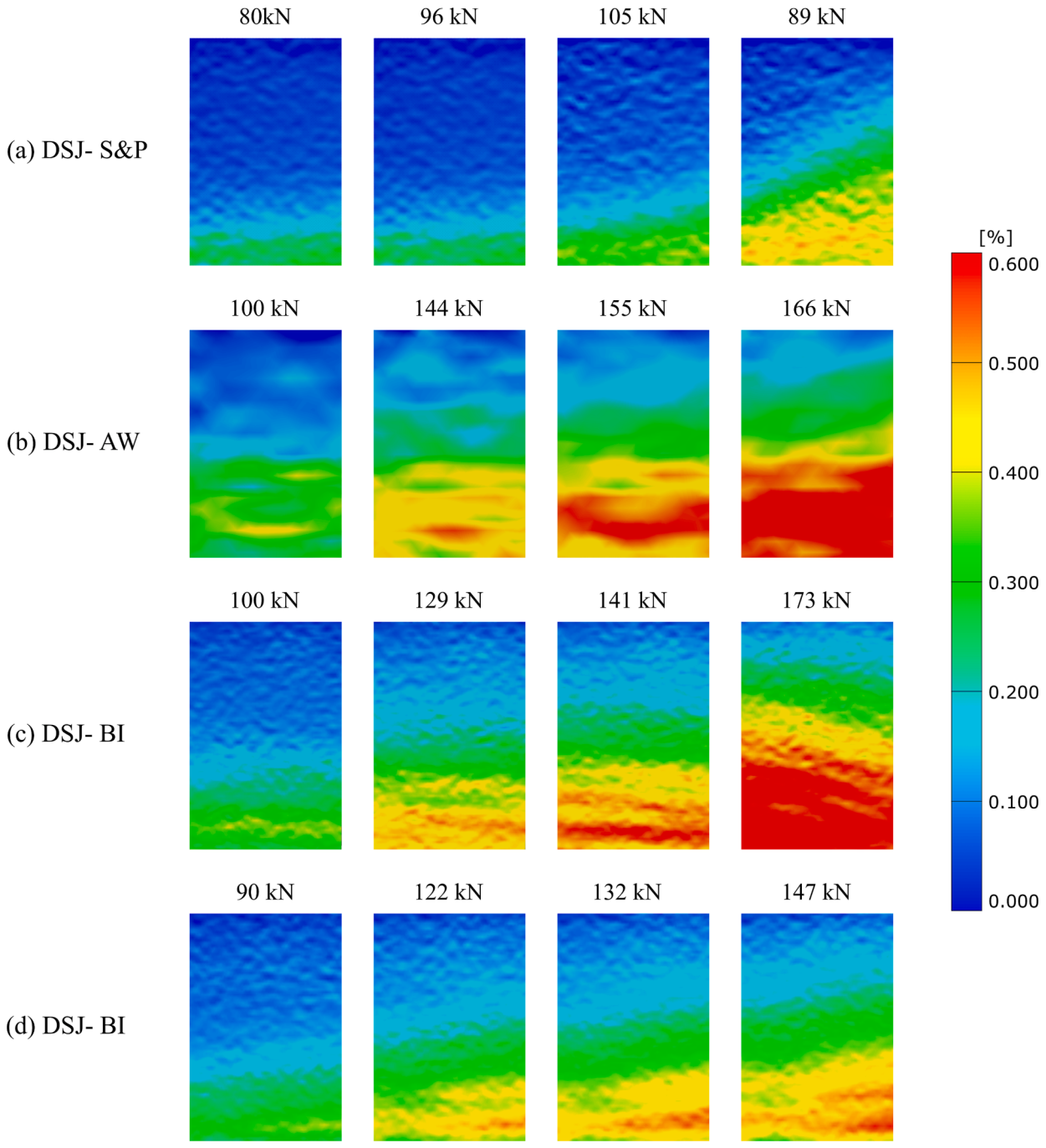

Fig. 8. Strain field distribution on the CFRP back face for the double strap joints with the different adhesives measured using DIC. From the middle of the joint (the bottom edge) to the free end of the overlap (top edge).

especially designed for bonding composites. It has high peeling resistance and shear resistance. For more information see the manufacturer datasheet [43].

Coupon tensile tests were conducted according to ASTM D638-14 [44] with specimens' geometry category 5 which is recommended for comparison between different adhesives. The specimens were made in acrylic molds and cured at room temperature for at least 7 days. The tests were conducted in the MTS 831–02 Elastomer test system with a speed of 1 mm/min. The strain measurements were acquired using an extensometer. The basic average material properties of the adhesives are presented in Table 1. Fig. 1 illustrates the stress–strain curves of the three different adhesives. The adhesive SK30 reached high strength (above 35*MPa*) and high stiffness but very low strain capacity (up to 0.3%). The adhesive S&P has a lower stiffness than SK30 and reaches roughly similar strength but with doubled deformation capacity. The adhesive AW has lower Young's modulus than the two brittle adhesives but higher deformation capacity and achieves similar strength around 35*MPa*. The toughness measured as the area under the stress–strain curve is extremely higher for the tough adhesive than the two other brittle ones.

Unidirectional pultruded CFRP laminates C-Laminate HM (200/2000) produced by S&P reinforcement® were used in this study. According to the datasheet provided by the manufacturer [45], the laminates are made with fibre volume content > 68%. The basic mechanical and geometrical properties provided by the manufacturer are presented

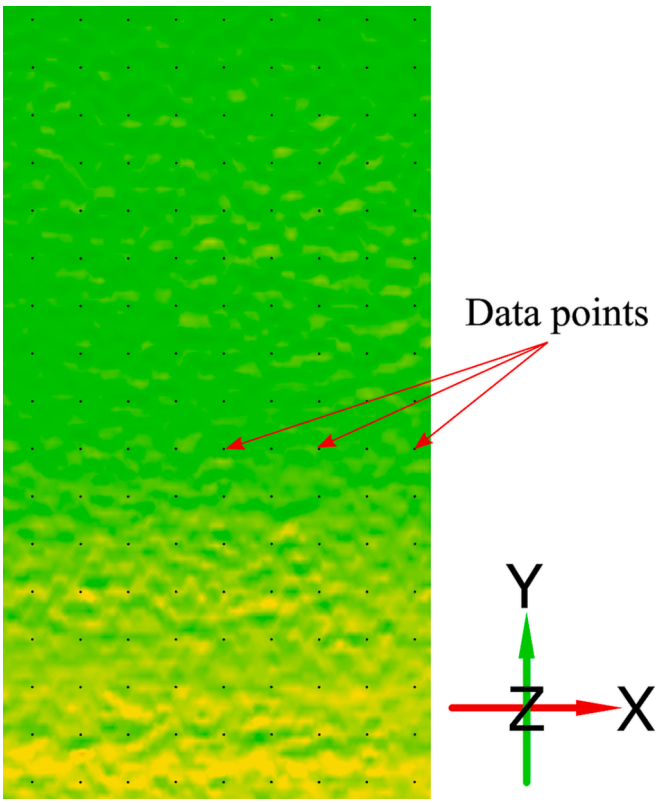

Fig. 9. Measurement data points.

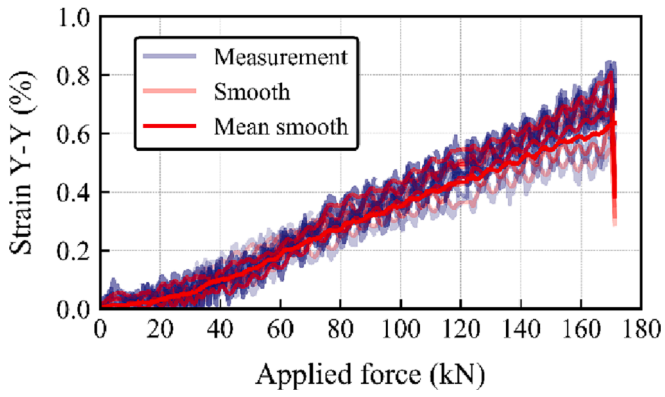

Fig. 10. Deformation in the Y-Y direction for DSJ-AW of the row near the joint versus the applied force.

in Table 2.

The steel bars were made of European hot rolled carbon steel S275 featuring a width of 50*mm*, thickness of 10*mm*, and a length of 500*mm*. The yields stress, Young's modulus, and ultimate stress are 350*MPa*, 200*GPa*, and 439*MPa*, respectively, as shown in related experimental study [6].

2.2. CFRP/steel double strap joints (DSJ)

The double strap joint consists of two separate steel bars joined together with a bonded CFRP patch in both sides, as shown in Fig. 2. Joints with single adhesive and bi-adhesive were manufactured and experimentally tested under tensile loading in this study. Each set of specimens consisted of at least 5 repeated tests. A schematic drawing of the specimens with single adhesive double strap joints is shown in Fig. 2 (a). Bi-adhesive joints were manufactured using a combination of tough (ductile) and brittle adhesives as shown in Fig. 2 (b). The internal transversal faces of the steel bars near the gap of the joint were smeared gently with unmolding agent to avoid butt joint effect. The two different adhesives were applied separately with an intended length distinguished by a letter "*d*" which represents the length of the tough adhesive taken equal to 10*mm*. The bi-adhesive specimen is made of the brittle adhesive S&P and the tough adhesive AW. The choice of the brittle adhesive S&P instead of SK30 was taken based on the experimental results of single adhesive DSJ joints where specimens with S&P showed a higher performance than the once with SK30 [23], as it will be shown in the subsequent sections. The fabrication of the DSJ specimens was made to ensure an adhesive thickness of approximately 1*mm* for all the specimens.

For single adhesive joints, the specimens are distinguished based on the adhesive used, where the nomenclature is presented in the form "*DSJ-Adhesive type*". For example, a double strap joint with adhesive SK30 or with bi-adhesive are named as: "DSJ-SK30" and "DSJ-BI", respectively.

2.3. Specimens' manufacture

The preparation of the specimens involved mainly two steps: (a) surface preparation of the steel and CFRP and (b) application of the adhesive between CFRP and steel in the mould. The surface preparation is a key step for the successful bonding of structural adhesives [46]. A proper surface treatment provides a rough surface favoring mechanical interlocking between the adherends and the adhesive to further increase the adhesion strength. The steel plates were sand blasted using alumina dioxide sand F60 with grain size between 212 and 300 micro, as recommended in [15], to avoid premature adhesion failure in the steel-adhesive interface. Then, the specimens were cleaned with compressed air and acetone to remove any particles left from the sand-blasting operation. The CFRP surface was gently polished in the fibre direction with sandpaper grit 180. Then, the CFRP plates were cleaned with compressed air and acetone.

The specimens were made in aluminium moulds, as shown in Fig. 3. The moulds are made of two thick flat aluminium plates of 25 mm thickness, 1300 mm long and 250 mm width. Each mould can accommodate 4 specimens in the longitudinal direction separated by pins. The main role of the pins is to ensure that the CFRP and the steel bars are well aligned. Aluminium spacers of 2.4*mm*were used to maintain a constant adhesive thickness of 1*mm*. After closing the mould the upper plate will apply a uniform pressure on the specimens. Then, the specimens were left to cure for at least 7 days at room temperature.

To control the overlap of the two adhesives in bi-adhesive joints a metallic rod of 1*mm* diameter was used during the application of the adhesives. The adhesives were smeared meticulously on the CFRP surface to maintain a 1*mm* thickness using the rods as reference. The rods were removed just before placing the CFRP on the surface of the steel plates. Keeping the rods would create crack-like defects that would negatively influence the strength of the joint [47]. Other researchers [39] used silicone rubber that could effectively sperate the adhesives however this methodology is recommended only for long overlap adhesive joint in which the area occupied by the rubber does not influence the joint strength [47]. The methodology applied in this study is similar to Pires et al. [48] which consists of calibrating the adhesive thickness as much as possible before bonding the CFRP and no physical barrier is applied between the adhesive.

2.4. Experimental set-up

Fig. 4 shows the experimental set-up adopted in this study. The DSJ specimens tested in ESH machine with a capacity of 1000*kN* in tension. The specimens were subjected to quasi-static tensile loading until complete failure. The loading speed was 1*mm*/*min*. The strain fields on

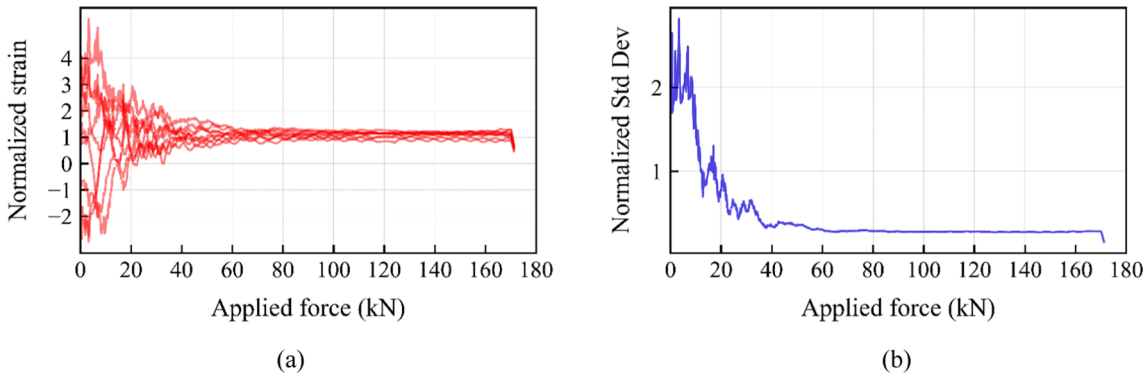

Fig. 11. Normalized strain (i.e. measured strain/mean strain) of 9 horizontal data points in the middle of a DSJ-AW joint: (a) Normalized strain versus applied force, (b) Standard deviation of the normalized strain versus the applied force.

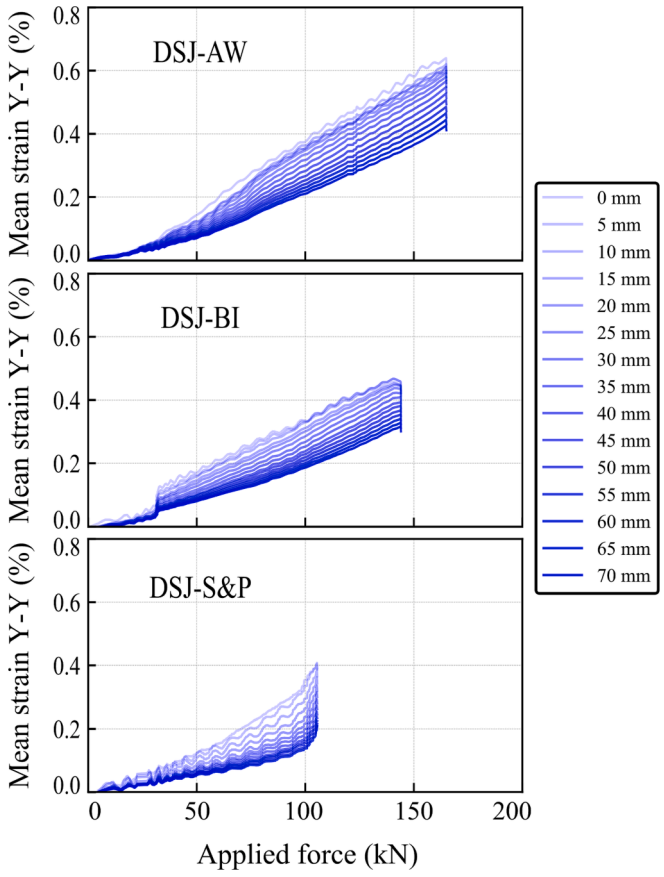

Fig. 12. Mean smoothed strain measurements on the CFRP back face at different locations from the middle of the joint. (Note: for DSJ-S&P the strain is measured up to 60 mm distance).

the back face of the CFRP plates were captured using 2D digital image correlation (DIC). A random speckle pattern with black background and white spots was applied on the back face of the CFRP or at the lateral face of the joint. Note, a maximum of 100 mm lens imaging was available so the lenses were controlled to achieve a sharp focus only on half of the joint, as shown in Fig. 4. Only one specimen was used to measure the strains on the lateral face of the joint however this methodology was stopped due to the high scatter of the results, see section 3.4 for more details.

3. Experimental results and discussion

3.1. Load displacement curves

Fig. 5 presents the load displacement curves of DSJ specimens bonded with CFRP using the different adhesives and configurations. For specimens DSJ-SK30, the strength reached a value between $65-85kN$ followed by a moderate flat plateau in most cases. The flat plateau has been reported in other studies in the literature [7] when cohesive failure is observed for joints with Sikadur 30. The maximum strength is associated with the crack initiation in the middle of the joint and the flat plateau is attributed to the crack propagation which depends on the length of the bonded area. Note the voids are inevitable in adhesive joints and their volume and location have a significant influence on the crack initiation and propagation in the adhesive joint, which justifies the variability of the experimental results. DSJ-S&P specimens reached a strength that fluctuates between $100-110kN$, followed by an abrupt failure due to delamination failure mode. DSJ-AW specimens reached a strength between $150-168kN$, which is very close to the measured average yield strength of the steel bar (See previous related study conducted by the authors ref. [23]). The DSJ-AW specimens failed under CFRP delamination, which is known as a brittle failure. The excessive yielding observed in the specimen that exhibited a long flat plateau is attributed to plastic deformation of the steel bars since the yield strength was reached as it was shown in a previous related study [23]. Whereas the behaviour of the others that showed limited ductility will be verified numerically in the subsequent section. DSJ-BI specimens reached a strength in a range of $145-175kN$. The high variability of the results might be due to some internal voids and the non-uniform distribution of the tough adhesive through the width.

Fig. 6 compares the joint strength of the specimens made with the different adhesives with respect to the yield strength of the base material. DSJ specimens with brittle adhesives (i.e. DSJ-SK30 and DSJ-S&P) reached an average strength of $76kN$ and $104.9kN$ with standard deviations of $\sigma = 6.02kN$ and $4.22kN$, respectively. The DSJ-AW specimens reached higher average strength of $160kN$ and a standard deviation of $\sigma = 6.09kN$. DSJ-BI achieved an average strength of $154kN$ with $\sigma = 12kN$. Clearly, the bi-adhesive configuration proposed in this study improved the joint strength significantly compared to the brittle adhesive alone. Compared to DSJ-S&P, an average of 46% improvement could be achieved when using bi-adhesive joints. The design yield stress of S275 steel is $275MPa$ which is the minimum value required to the steel producers to qualify the steel as S275, in practice all the structural design checks need to be done using this value. However, the actual experimentally measured yield stress was $350MPa$. For the steel bars of $50x10mm$ used in this study, the design strength (i.e. $Crosssectionarea \times Designyieldstress$) and measured strength (i.e. see ref. [23]) become $137kN$ and $175kN$, respectively. As shown in Fig. 6, the design yield

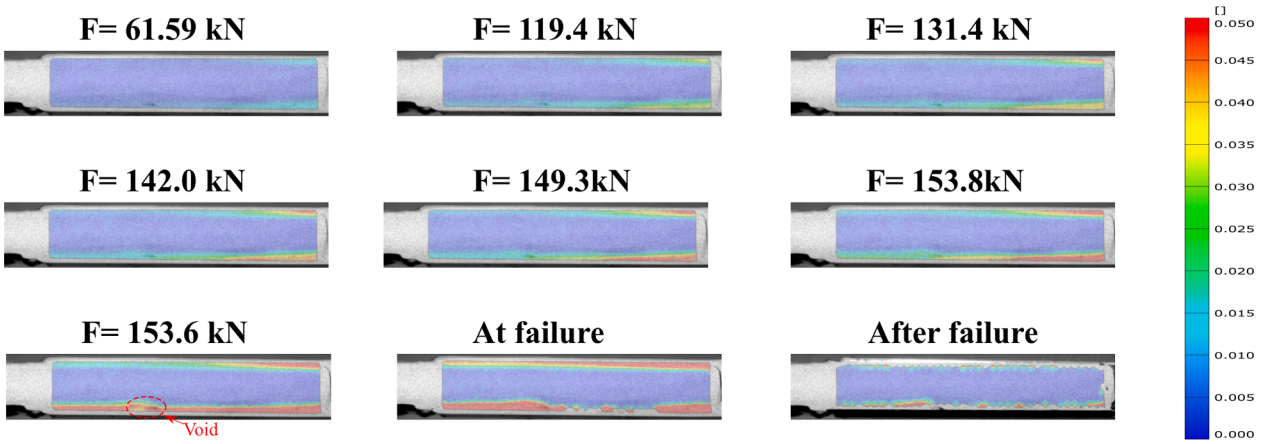

Fig. 13. Equivalent strain distribution in the adhesive layer of specimen with AW4858/HW4858 adhesive using DIC.

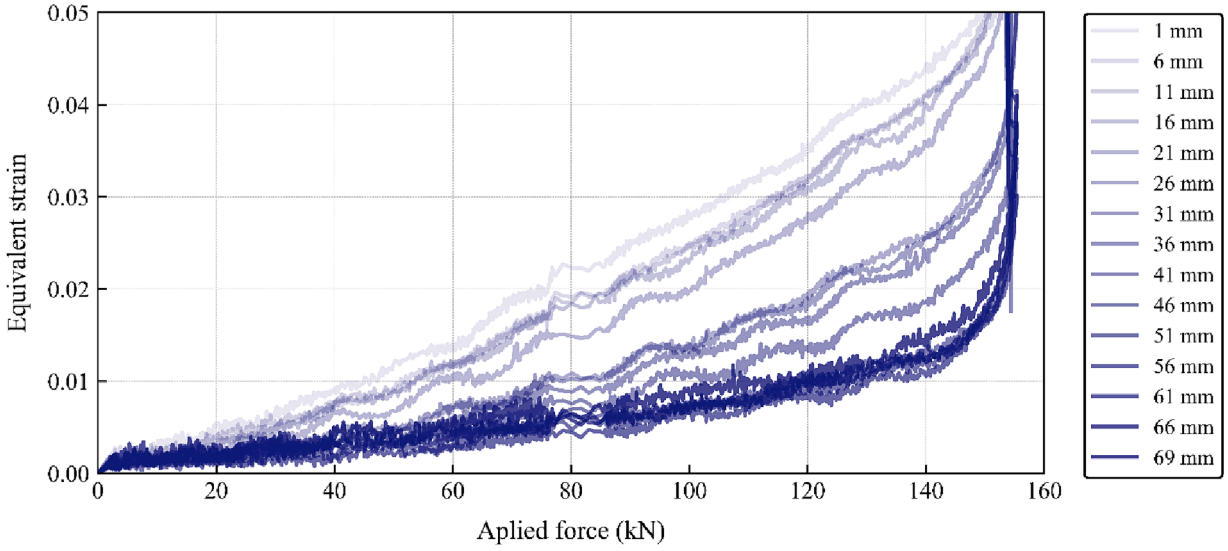

Fig. 14. Equivalent strain at different points from middle of the joint versus applied force.

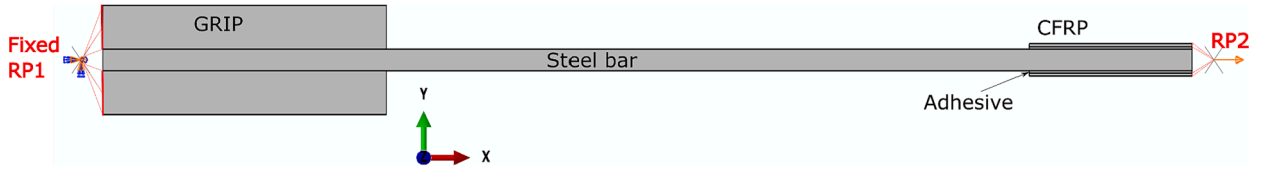

Fig. 15. A schematic view of the numerical model.

Table 3
Steel material elastoplastic model input parameter (also published in [6]).

Material	Elasticity		Plasticity	
	Elastic modulus (GPa)	Poisson ratio	Yield stress (MPa)	Plastic strain
Steel	200	0.3	350 370 440,500	0 0.022 0.05170.1

Table 4
Adhesive elastoplastic model input parameters (also published in [6]).

Material	Elasticity		Plasticity	
	Elastic modulus (GPa)	Poisson ratio	Yield stress (MPa)	Plastic strain
AW	1.32	0.35*	35.536	00.15
S&P	7.6	0.35*	N.A.	N.A.

* Assumed parameter.

strength of the steel bars was exceeded for specimens with tough adhesive and bi-adhesive configuration. From a design point of view, the adhesive joint in these DSJ specimens is stronger than the design strength of the parent material, thus, the specimens reached a joint strength efficiency of 100%. As it was shown in ref. [23], the joint strength efficiency can be used for the design of composite patches stronger than the parent material without the need to carry out cumbersome design checks on the fracture of the adhesive layer or the

Table 5
Engineering elastic constants for the material model used to model the CFRP.

Case	$E_1(GPa)$	$E_2(GPa)$	$G_{12}(GPa)$	ν_{12}
Anisotropic 1	205	3.7	5.29	0.286
Anisotropic 2	205	12.79	5.29	0.286
Isotropic	205			0.3

CFRP, which is very complex. So further development of design rules based joint efficiency are higher recommended.

3.2. Failure modes

The failure modes and the inspection of the fracture surface provide important information on the behaviour of the adhesive joint. According to Majidi et al. [49], the possible mode of failures in the steel/CFRP joint are the followings: Adhesive failure at the adherends-adhesive interface caused usually by inadequate surface treatment [46], cohesive failure in the adhesive layer, CFRP rupture that occurs for high modulus CFRP due to its limited deformation capacity [50], CFRP delamination, and steel yielding. Fig. 7 (a) illustrates two typical DSJ-SK30 specimens, where the failure mode is a combination of cohesive failure within the adhesive and CFRP delamination occurring at the free ends of the overlap, where peel stresses are higher. Similar observations have been reported in Ref. [7] for specimens with SK30 adhesive. Fig. 7 (b) illustrates the typical failure mode for DSJ-S&P specimens which consists mainly of CFRP delamination with small areas affected by cohesive failure. Fig. 7 (c) illustrates the typical failure mode for DSJ-AW specimens, where the failure mode is CFRP delamination. For DSJ-BI, the main failure mode is CFRP delamination with limited cohesive failure in the region of the S&P adhesive, as shown in Fig. 7 (d).

The failure in the composite patch is a crack that initiates and propagates in the component that satisfies the Griffith energy criterion $G > G_c$, where G is the energy demand on the material and G_c is a material property called critical strain energy release rate. The delamination failure mode occurs due to a crack in the CFRP matrix. The failure mode observed in this study were either cohesive or CFRP delamination. When the adhesive is tougher than the CFRP matrix, the failure mode occurs in the CFRP and vice versa. This can be clearly observed in these experimental results, where cohesive failure governed the failure mode for DSJ-SK30 specimens that were made with a low toughness adhesive (i.e. SK30). Whereas for DSJ-AW specimens made with the tough adhesive AW, CFRP delamination was the failure mode. For DSJ-S&P specimens made with S&P adhesive, which is moderately tougher than SK30, a combination of CFRP delamination and limited cohesive failure governed the failure mode.

3.3. Strain distribution

Fig. 8 shows the strain fields at different levels of loading on the back face of the CFRP captured using DIC on specimens with the brittle adhesive (DSJ-S&P), the tough (DSJ-AW), and bi-adhesive (DSJ-BI). Note the strain fields are captured only on half of the CFRP face from the middle of the joint (bottom part) to the free edge, as shown in Fig. 4. The DSJ-S&P specimen shows a concentration of deformation in the middle of the joint which tends to propagate at larger loading levels, but the strains are not uniformly distributed which may indicate the presence of a weaker zone due to manufacturing imperfections such as voids. The DSJ-AW specimen exhibits deformation at almost all the areas especially at the highest loading level before failure. Fig. 8 (c) and (d) show two DSJ-BI specimens, where one reached very high strength ($173kN$) and the other the lowest strength ($147kN$). In general, DSJ-BI specimens show strain levels and fields distributed on larger areas than DSJ-S&P. The DSJ-BI shown in Fig. 8 (c) experiences very large deformation levels comparable to DSJ-AW, which justifies the higher strength reached (see Fig. 5). The DSJ-BI shown in Fig. 8 (d) shows a non-uniform strain fields distribution and much lower deformation levels before failure which occurred at relatively lower strength. This was due to a large void located near the middle of the joint region, as shown in Fig. 7 (d).

The contour plots presented in Fig. 8 provide a good insight on the behavior of the adhesive joint. However, due to the large scatter, it does not provide a clear quantification of strains along the CFRP which can be used for the development of strength models such as the bond-slip model [51]. In previous studies, the strain measurement along the CFRP length was obtained using strain gauges bonded on the CFRP back face [51–53]. In this paper, a methodology based on the DIC measurements is adopted to evaluate the strains. The noise is an inherent aspect of the DIC technique which can be clearly seen in Fig. 8. To tackle this issue,

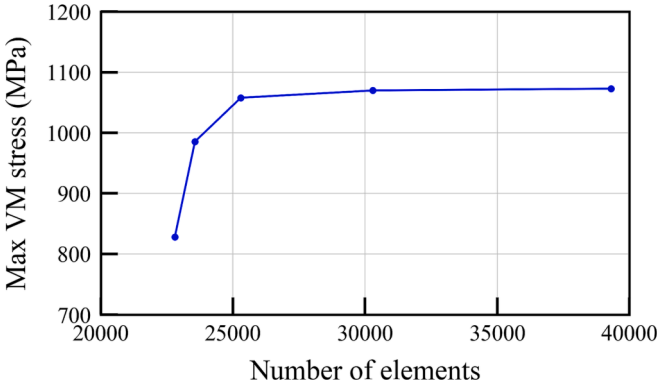

Fig. 17. Mesh sensitivity study.

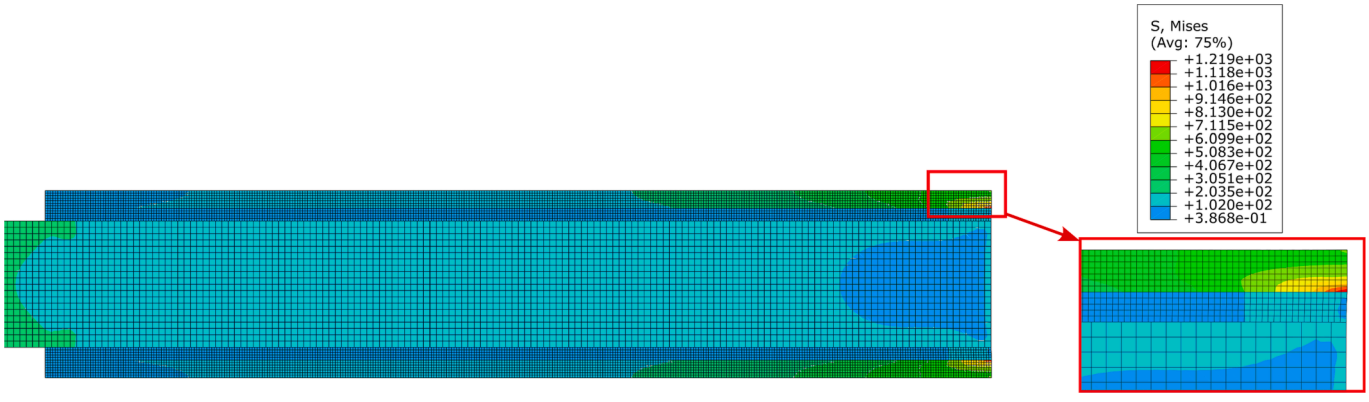

Fig. 16. Stress concentration due to discontinuity at the CFRP/adhesive interface.

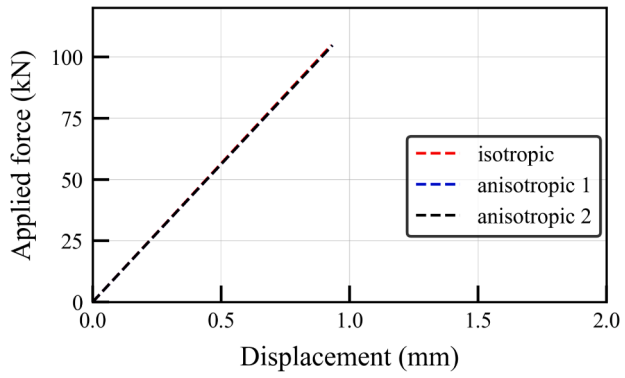

(a) Force displacement

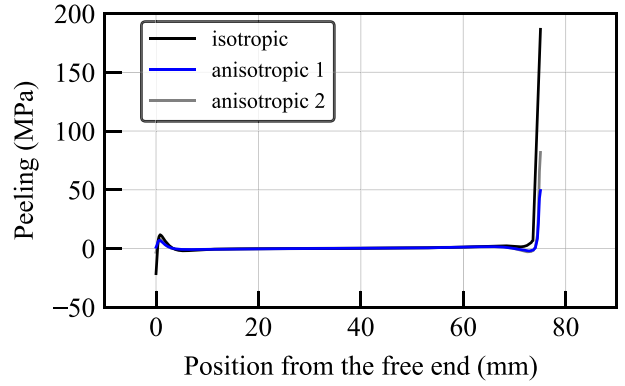

(b) Peeling stress in the CFRP at the CFRP/adhesive interface

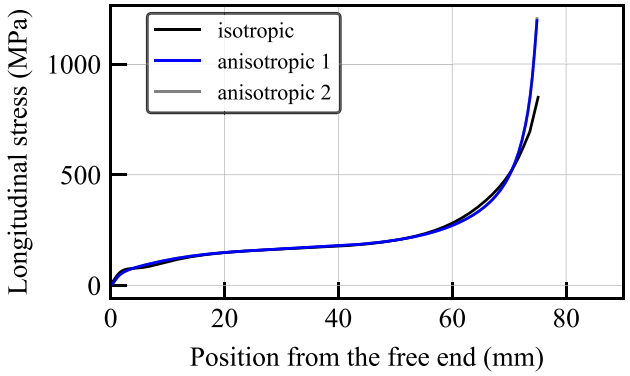

(c) Longitudinal stress in the CFRP at the CFRP/adhesive interface

Fig. 18. The influence of the material model of the CFRP on the DSJ joints.

the strain measurements were made from data points spaced by 5 mm apart in the horizontal and vertical directions, as show in Fig. 9, where each row represents the behavior at a given distance from the middle of the joint. Fig. 10 shows an example of the strain data at the joint level. The row data show significant noise within each data point. In order to reduce the fluctuations within each line, the data was smoothed giving the discrete linear convolution of two, one-dimensional sequences. Then, the average was calculated based on the smoothed data. Note the inline fluctuation are assumed to be the noise from the DIC measurements but the differences between the smoothed lines in the same row is assumed to be due the different behavior between each point, as obviously shown in Fig. 8 (a) for specimen DSJ-S&P at 89*kN* of applied load. The possibility of capturing the variation of deformation levels along the width makes the use of DIC particularly advantageous in this application since this cannot be feasibly obtained using strain gauges as adopted in previous studies.

In Fig. 11 (a), the normalized strain (i.e. measured strain/mean strain) shows high variability at loading lower than 60*kN* then the data tend to converge toward 1. Fig. 11 (b) shows the standard deviation of the normalized strain, where it shows that there is a high variation at lower loading levels and then reduce to 0.13. This indicates that the use of DIC technique at low strain levels would be more challenging to provide accurate results due to the significant noise. This is the case of specimens DSJ-SK30 which is not shown in here for brevity.

Fig. 12 presents the mean strain versus the applied loading curves along the CFRP back face length (spaced by 5 mm) for the DSJ-S&P, DSJ-AW, and one DSJ-BI that was shown in Fig. 8 (d). Clearly, the DSJ-AW exhibits large deformation above 0.6% at the middle of the joint before failure. The DSJ-BI shows a relatively large deformation with maximum value of 0.48%. The curves of the DSJ-BI show a step at 30 *kN* of applied force. This was due to a local premature damage that happened next to the middle of the joint due to a large void as shown in Fig. 7 (d). DSJ-S&P exhibits relatively lower deformation levels with a maximum value of 0.4% at the middle of the joint but very low deformation at the free edge of the joint, where strain could be captured only up to 60 *mm* distance from the joint with a value of 0.2%.

3.4. Failure pattern assessment using DIC

Fig. 13 presents the evolution of the equivalent strain on the lateral face of the CFRP/Steel adhesive joint obtained using DIC. The strain fields in the thickness of the CFRP could not be captured by the software due to significant noise. It should be noted that it is very challenging to analyze and obtain precise results in the adhesive layer [34]. Inhere the strain fields are provided for qualitative analysis only. Referring to Fig. 13, the strain fields increase in intensity and cover a larger area as the loading increases. The failure of the specimen initiated in the most stressed area at the middle of the joint. The behavior of the joint shows unsymmetric behavior, where the lower adhesive layer is subjected to higher deformation levels. This can be also observed in a similar test conducted by Haghani [28]. It might be due manufacturing imperfections or defects such as voids in the adhesive layer as highlighted in the figure. Voids are an inherent nature of bonded joints, it is impossible to manufacture a bonded joint free from voids [26]. As whether these defects are critical depends on their extent, position, and the nature of the applied stress. Wang et al [54] tested epoxy bonded lap joints with inserted large defects and showed that the joint strength little changed.

Fig. 14 shows the evolution of the (Von Mises) equivalent strain versus the applied loading along the adhesive layer length. The measurements are taken from equally spaced aligned points (5 mm) on the adhesive layer. The level of deformation is higher for data points closer to the middle of the full joint (Near the gap), except at the end of the overlap, where in the last two points at (69*mm* and 64*mm*), the equivalent strain slightly increases due to peeling deformation.

From Fig. 8 and Fig. 13, the failure initiates and propagates from the middle of the joint (Near the gap) until reaching the complete failure.

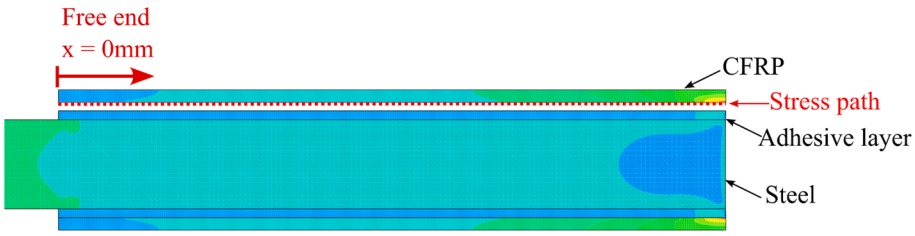

Fig. 19. Stress Path in the CFRP at the CFRP/adhesive interface.

This gives indication that the peeling stress at the end of the CFRP does not have a contribution to the crack initiation. In the middle of the joint, the adhesive layer is mainly subjected to shear. This behavior is different from the ubiquitous single lap joints, or the double strap joints [55] with very short overlap used in the aerospace structure crack repairs, where the effect of peeling stress can be significant. Indeed, this was the main reason for the development of the bi-adhesive configuration proposed in this study. The strengthening strategy of the DSJ joint is fundamentally different from previous studies. Inhere, the tough adhesive is placed in the middle of the bi-adhesive joint to contribute mainly in shear and allow a relatively more uniform distribution of shear stresses along the joint compared to adhesive layer with brittle adhesive alone. The results presented in this paper show that the use of new configuration of bi-adhesive joint where a tough adhesive is used in the region shear stress concentration can provide a significant improvement in strength.

4. Numerical analysis

4.1. Development of the F.E model

A 2D Finite element model was developed in the commercial software ABAQUS to simulate the behaviour of DSJ specimens tested experimentally. Only half of the joint was modelled due to symmetry. The model is shown in Fig. 15, which consists of a steel bar, adhesive layers, CFRP plates, and testing machine grips. Since yielding was observed in the load displacement curves of some specimens with the tough adhesive, the machine grips were also modelled in order to capture any stress concentration zone created by the compression of the grips. The numerical model has the same geometry and dimensions of the experimental specimens shown in Fig. 2.

Tie constraints were assumed between the grips and the steel bar to ensure no slip as in the experiment. A compression force of $1MN$ was uniformly applied on the grips as in the experiment. The steel material of the grips was assumed linear with $200GPa$. The free edge of the grips was constrained as a rigid body to a reference point "RP1" which was in turn restrained in all degrees of freedom to ensure fixed boundary conditions. The loading displacement was applied on the CFRP edge section as only half of the joint is modelled. The CFRP edge section was constrained as a rigid body to a reference point RP2 where the loading was imposed. The steel/adhesive and the CFRP adhesive interfaces were modelled with tie constraints where the adhesive surfaces were taken as slaves. The model developed in this study is mainly for supporting the discussion on the behavior of the joints tested experimentally. The simulation of damage is beyond the scope of this study as it requires additional fracture mechanics tests to calibrate the numerical damage models.

4.2. Materials

The elastic–plastic material behavior of the steel and the adhesives was modelled using isotropic model calibrated using experimental true stress–strain curves. The input data of the elastic–plastic model are presented in Table 3 and Table 4.

The CFRP used in this study is unidirectional. Hence, it is more appropriate to model the behavior of the CFRP using an orthotropic material model. However, due to the unavailability of experimental data, several research [20,56–59] that focused on double strap joints subjected to tensile loading assumed the CFRP as isotropic. Haghani [60] investigated the effect of considering orthotropic or isotropic for similar specimens and showed that the isotropic model gives acceptable results on the overall behavior. In this study, the CFRP is modelled using the two approaches for comparison. To model the anisotropy, the elastic orthotropic material model available in ABQUS library was adopted. The input parameters were obtained using the micro-mechanics model presented in ref. [61,62], which consists of:

$$E_1 = E_{f1}V_f + E_mV_m \tag{1}$$

$$E_2 = \frac{E_{f2}E_m\left(V_f + \eta_2 V_m\right)}{E_mV_f + E_{f2}\eta_2 V_m} \tag{2}$$

$$\eta_2 = \frac{0.2}{1-\nu_m}\left(1.1 - \sqrt{\frac{E_m}{E_f}} + \frac{3.5E_m}{E_f}\right)(1 + 0.22V_f) \tag{3}$$

$$G_{12} = \frac{G_fG_m\left(V_f + \eta_{12}V_m\right)}{G_mV_f + G_f\eta_{12}V_m} \tag{4}$$

$$\eta_{12} = 0.28 + \sqrt{\frac{E_m}{E_f}} \tag{5}$$

$$\nu_{12} = \nu_fV_f + \nu_mV_m \tag{6}$$

The subscripts "$m.f,1,2$" denote matrix, fibre, longitudinal direction, and transverse direction, respectively. Where, E_1, E_2, are the elastic modulus in the longitudinal and transversal direction of the composite laminate, respectively. The parameters G_{12} and ν_{12} are the shear modulus and the Poisson's ratio of the laminate, respectively. The fibre volume content ratio V_f of the laminate is presented in Table 2, whereas the matrix volume content ratio is taken as $V_m = 1 - V_f$. The CFRP used in this study is made with pultrusion process using high modulus CFRP fibres and Vinyl Ester matrix [63]. The manufacturer provides only the basic mechanical properties of the laminates such as the elastic modulus in the fibre direction "E_1", the ultimate strength, and elongation at break, as presented in Table 2. The mechanical properties of the fibres and the matrix are not provided. Therefore, the parameters are taken from the literature. The elastic modulus and the Poisson's ratio of the matrix are taken from [64], where $E_m = 3000MPa$ and $\nu_m = 0.3$, respectively. The axial Poisson's ratio of carbon fibres is taken as $\nu_f = 0.28$ [65,66] and the shear modulus $G_f = 15GPa$ [66,67]. The transverse elastic modulus of CFRP "E_{f2}" is usually between $4-14GPa$ [68]. In this study, the two extreme value of $E_{f2} = 4GPa$ and $E_{f2} = 14GPa$ are considered to check if the variability of these values has any influence on the behavior of the joint. The longitudinal elastic modulus of the fibres E_{f1} is calculated using equation (1) as E_1 is provided by the manufacturer. The input used in the orthotropic model as well as the isotropic model are presented in Table 2. In order to verify the sensitivity of the assumptions adopted for modelling the CFRP, three sets of input parameters are utilized, as shown in Table 5. Where:

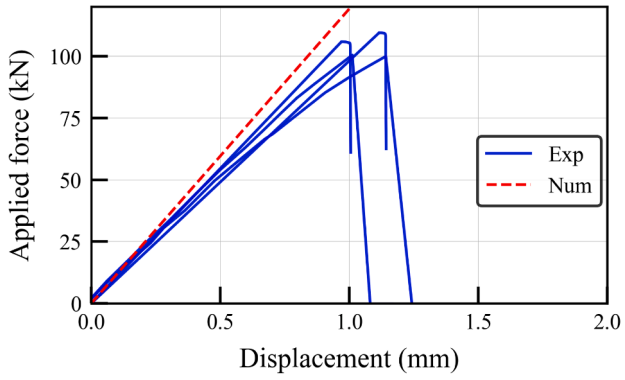

(a) DSJ-S&P

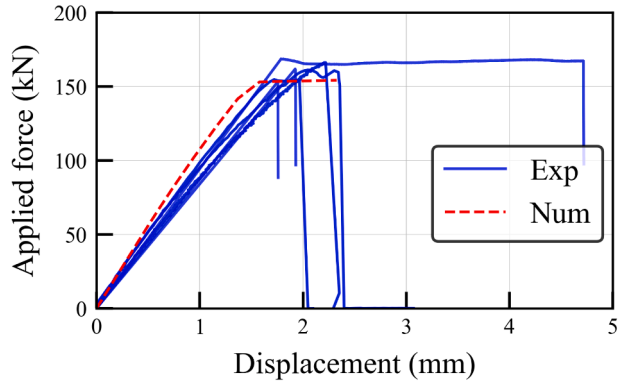

(b) DSJ-AW

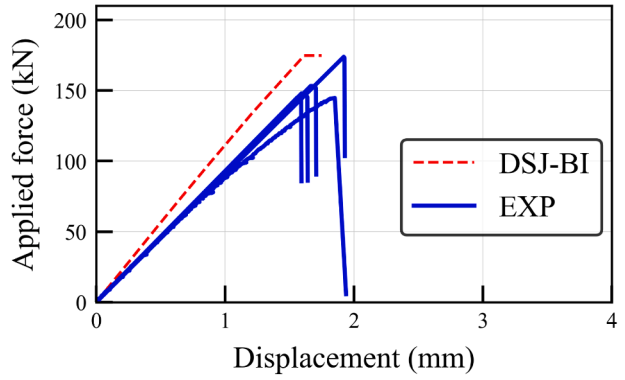

(c) DSJ-BI

Fig. 20. Comparison between experimental and numerical results.

- Anisotropic 1: the orthotropic material model is adopted assuming the transverse elastic modulus of the fibres is equal to 4*GPa*.
- Anisotropic 2: the orthotropic material model is adopted assuming the transverse elastic modulus of the fibres is equal to 14*GPa*.
- Isotropic: where the CFRP is assumed as isotropic.

4.3. Meshing

All the model was developed using plane stress linear quadrilateral elements CPS4R available in the software library. In order to obtain reasonably accurate results it is important to conducted a mesh sensitivity study [69]. This is more particularly important to calibrate damage models when they are considered in the simulation [70]. Although, modelling the damage is beyond the scope of this study, a mesh sensitivity analysis is conducted to ensure reasonably accurate stress and strains are obtained from the model especially at stress concentration zones, as shown in Fig. 16.

The most critical region is at the material discontinuity between the CFRP and the adhesive, as it is shown in Fig. 16. Therefore, the mesh sensitivity is conducted by varying the number of finite elements only at the CFRP and the adhesive. Note: The mesh size in the CFRP and the adhesive was always kept the same. Only one type of joint (i.e. DSJ-S&P) was considered for the mesh sensitivity study, where the joint was subjected to 105*kN*. The mesh size in the steel was kept constant equal to 0.5 mm. The Von Mises (VM) stress was obtained at the stress concentration point which is at the CFRP end near the CFRP/adhesive interface as shown in Fig. 16. Fig. 17 shows the evolution of maximum VM stress at the stress concentration point versus the number of mesh elements. As can be seen, after 30 300 elements, the maximum VM stress tend to converge toward the same value. Therefore, for the model with 30 300 elements corresponding to a mesh size od 0.2*mm* was adopted in the subsequent studies.

4.4. Influence of the CFRP material model and anisotropic input parameters

In this section, a comparison between the assumption of the isotropic model and the more realistic orthotropic model is presented. As stated previously two sets of anisotropic properties of the CFRP were assumed in the orthotropic model. The comparison is done only for DSJ-S&P specimens for brevity. Fig. 18 (a) shows the force displacement curves for DJS-S&P joints and Fig. 18 (b) and (c) illustrate the peeling and longitudinal stress along the stress path shown in Fig. 19, which is in the CFRP at the CFRP/Adhesive interface. From Fig. 18 (a), the force–displacement curve does not show any influence of the material model used for CFRP, both the isotropic and orthotropic model show similar results. However, Fig. 18 (b) and (c) show that the stress distribution at the CFRP/adhesive interface is different especially at position of maximum stress concentration. The joint with the isotropic model develops very high peeling stress (186*MPa*) which is mainly caused by the high transverse elastic modulus. The behavior of the CFRP laminate in the transverse direction is mainly governed by the matrix, which usually has a much lower tensile strength. For example the laminates used in this study are made with Vinyl Ester resin that can have a maximum tensile strength of 95*MPa* [64]. Therefore, the value reached using the isotropic is unrealistic. Whereas the use of the orthotropic model gives more realistic estimation of the peeling stress with values of 49.4*MPa* and 81.8*MPa* for anisotropic 1 and anisotropic 2, respectively. Fig. 18 (c) shows the distribution of the longitudinal stress in the CFRP/adhesive interface, where the joints with the orthotropic model exhibit higher maximum longitudinal stress than the joint with the isotropic model. Overall, it can be concluded that for the simulation the unidirectional CFRP behavior in the specific case of double strap joints subjected to tensile loading, the use of the isotropic or orthotropic models shows mainly important differences at the stress concentration zones where usually the damage initiation occurs. Therefore, it is crucial to include the anisotropy when damage models are included to simulate failure. However, when there is a lack of experimental data, the isotropic assumption can still give reasonable prediction of the behavior away from the stress concentration zone. In the subsequent studies, the orthotropic model is used in the numerical models considering the parameters anisotropic 1.

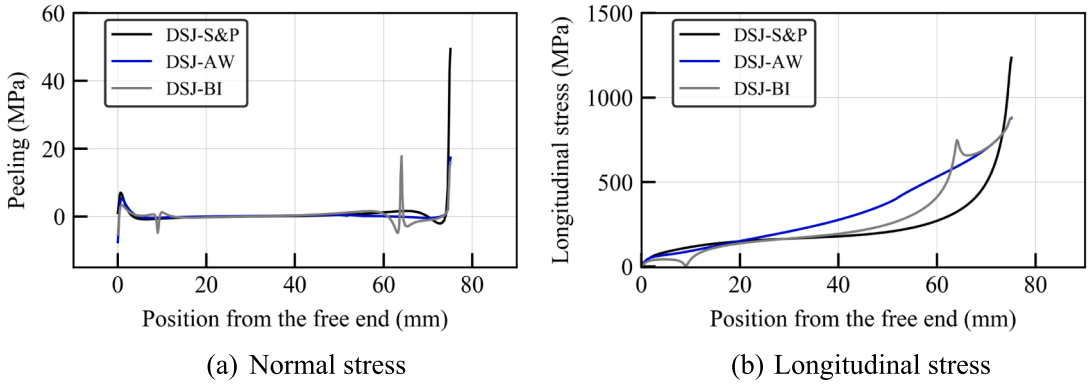

Fig. 21. Comparison between the stress distribution obtained numerically along the path shown in Fig. 18 for DSJ-S&P, DSJ-AW, and DSJ-BI.

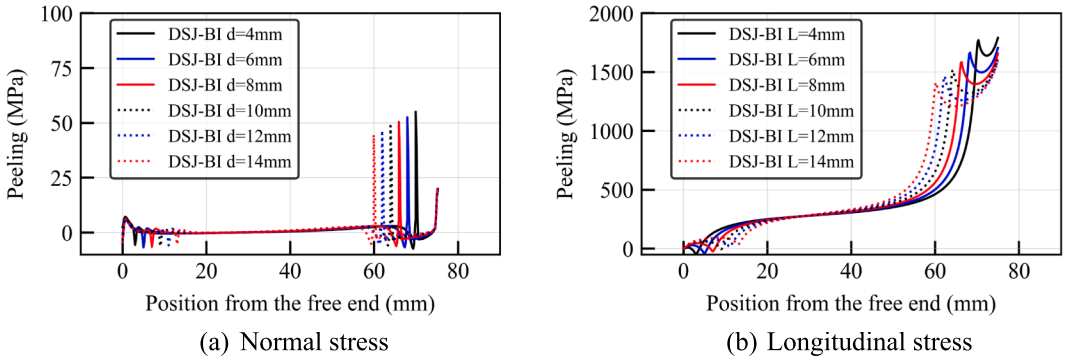

Fig. 22. Comparison between the stress distribution obtained numerically a long the path shown in Fig. 19 for DSJ-BI with different ductile adhesive length.

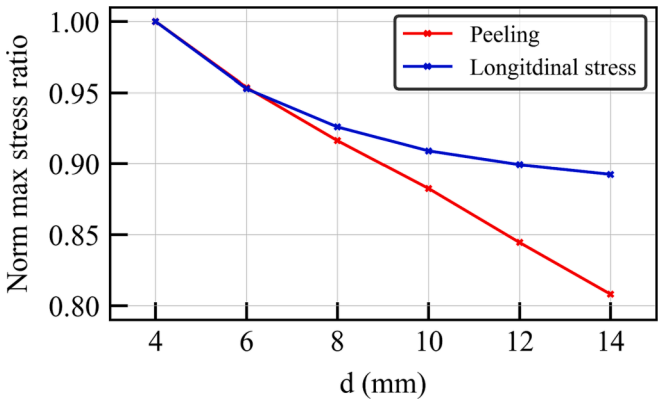

Fig. 23. Reduction of maximum stress versus the length "d" in DSJ-joints.

4.4.1. Comparison between numerical and experimental results

Fig. 20 shows that the comparison of the numerical and the experimental results for DSJ-AW, DSJ-S&P, and DSJ-BI. As can be seen, the numerical results match fairly well the experimental data. As stated previously, the failure of the joint or any damage in the joint components is beyond the scope of this study. The DSJ-AW numerical model reached a maximum strength of $152kN$ where the adhesive experienced yielding in shear. At the steel bar, the maximum stress is almost $340MPa$ which represents 97% of the experimental yield stress. At this stage the steel did not experience any plastic deformations, as it was shown in a previous related study [23], where it was shown that the DSJ-AW specimen among others that experienced significant yielding (i.e. with a long flat plateau), the steel have yielded.

4.4.2. BI-adhesive joint

Fig. 21 shows the normal and the longitudinal stress along the path shown in Fig. 19 for DSJ-S&P, DSJ-AW, and DSJ-BI. As can be seen, DSJ-S&P numerical model exhibits higher peeling stress than the joint DSJ-AW. The longitudinal stress in DSJ-S&P shows higher level of stress concentration near the joint region whereas DSJ-AW experiences a more distributed stress and much lower intensity. For DSJ-BI, both the longitudinal stress and the peeling stress are reduced significantly compared to the joint with brittle adhesive DSJ-S&P. The longitudinal stress distribution exhibits a peak at the middle of the joint coincident with the peak of the DSJ-AW and at the interface between the brittle and the ductile adhesive. The peeling stresses are also reduced significantly at the middle of the joint.

Fig. 22 shows the influence of the length of the ductile adhesive "d" on the stress distribution at the CFRP/adhesive interface for DSJ-BI joints. The length "d" was varied between $4-14mm$. As can be seen, the maximum peeling stress as well as the longitudinal stress tend to decrease with the increase of "d". The highest stresses are observed at the lowest value of "d" which is equal to $4mm$. Fig. 23 shows that the variation of the normalized maximum peeling and longitudinal stresses with respect to the length "d" in DSJ-BI joints. The normalized maximum stress is calculated as the ratio between the maximum stress for a joint with a given "d" divided by the maximum stress in a joint featuring a $d = 4mm$. Where for a DSJ-BI with $d = 4mm$, the normalized maximum stress is equal to 1. From Fig. 23, the normalized longitudinal stress curve shows a parabolic shape where a maximum decrease of stress is achieved at $d = 14mm$, with a ratio of 0.107. Considerable decrease of longitudinal stress can be observed between $d = 4mm$ and $d = 10mm$, whereas the difference in ratio between $d = 10mm$ and $d = 14mm$ is only 0.01 6. The peeling stress decreases linearly with the increase of "d", with the maximum decrease reached at $d = 14mm$ with a difference of 0.192. Overall, it can be concluded that within the range of "d" lengths considered in this study, the influence of the length "d" remains below

20% of the maximum stress. Although this might affect the result, the influence of the length remains within the scatter band usually observed in adhesive joint with a single adhesive.

5. Conclusion

This paper presents a new high performance CFRP/Steel joint using hybrid bi-adhesive technique for the repair of metallic infrastructures. Experimental testing of double strap joints was conducted to compare the performance of CFRP/Steel joints bonded with brittle adhesives commonly used in related research, an extremely tough adhesive and the proposed bi-adhesive joint. The results revealed that the tough adhesive provide much higher performance and is more suitable for bonding on metallic components. However, the cost of the tough adhesive can be significantly higher than brittle ones and may question its feasibility in the construction industry as large amounts of adhesive are required. Therefore, the bi-adhesive CFRP/Steel joint that uses small amounts of the tough adhesive combined with the brittle adhesive is proposed as a cost-effective alternative. Experimental and finite element investigations revealed that:

- The proposed bi-adhesive CFRP/steel joint reaches very high strength comparable to the strength of the CFRP/steel joints with tough adhesive alone.
- Specimens with brittle adhesives showed a combination of cohesive and delamination failure mode. The Specimens with tough adhesive showed only delamination of the CFRP as the fracture toughness of the adhesive is very high, the weakest part became the CFRP. Bi-adhesive DSJ specimens failed mainly in delamination failure mode with limited cohesive failure in the region of the brittle adhesive.
- Strain field distributions obtained using DIC showed that the damage initiates from the middle of the joint and the role of the tough adhesive in bi-adhesive joint is mainly in reducing shear stresses which is different from existing configurations of bi-adhesive joints. This was also demonstrated from the finite element analysis.
- The use of the tough adhesive promotes a more uniform strain distribution on the back face of the CFRP back face.
- The bi-adhesive configuration proposed in this study seems to be a cost effective compared to the tough adhesive alone. However, this paper shows only the concept, more studies are needed to proof its applicability for real applications including specifically the durability for variable environmental conditions.
- The numerical results revealed that the influence of the proportion of the ductile adhesive and rigid adhesive in bi-adhesive joints on the maximum stress remains below 20%.

CRediT authorship contribution statement

Anis Mohabeddine: Conceptualization. **Ghassan Malik:** . **José Correia:** Validation, Supervision. **Abílio De Jesus:** Validation. **Nicholas Fantuzzi:** Validation, Supervision. **José Miguel Castro:** Validation, Supervision.

Declaration of Competing Interest

The authors declare that they have no known competing financial interests or personal relationships that could have appeared to influence the work reported in this paper.

Data availability

Data will be made available on request.

Acknowledgments

This research was funded by the FiberBridge project - Fatigue strengthening and assessment of railway metallic bridges using fiber-reinforced polymers (project grant POCI-01-0145-FEDER-030103 composed by FEDER funds provided by COMPETE2020 (POCI) and by national funds (PIDDAC) provided by the Portuguese Science Foundation (FCT/MCTES)). Support was also provided by CONSTRUCT - Instituto de I&D em Estruturas e Construções that is funded by base funding - UIDB/04708/2020 and programmatic funding - UIDP/04708/2020 provided by national funds through the FCT/MCTES (PIDDAC). José A.F.O. Correia would like to thank the individual project grant (2020.03856.CEECIND) awarded by national funds (PIDDAC) through the Portuguese Science Foundation (FCT/MCTES).

The authors gratefully acknowledge S&P reinforcements (Portugal) for supporting this research.

The authors gratefully acknowledge SIKA (Portugal) for supporting this research.

The authors gratefully acknowledge Huntsman Advanced Materials (Switzerland) for partially supporting this research.

References

[1] Mohabeddine A, Correia JAFO, Montenegro PA, Castro JM. Fatigue crack growth modelling for cracked small-scale structural details repaired with CFRP. Thin-Walled Struct 2021;161. https://doi.org/10.1016/j.tws.2021.107525.
[2] Kasper Y, et al. Application of toughened epoxy-adhesives for strengthening of fatigue-damaged steel structures. Constr Build Mater 2021;275:121579. https://doi.org/10.1016/j.conbuildmat.2020.121579.
[3] Mohabeddine A, et al. An approach for predicting fatigue life of cfrp retrofitted metallic structural details. Int J Fatigue 2021:106557. https://doi.org/10.1016/j.ijfatigue.2021.106557.
[4] Mohabeddine A, Correia J, Aires Montenegro P, De Jesus A, Miguel Castro J, Berto F. Probabilistic S-N curves for CFRP retrofitted steel details. Int J Fatigue 2021;148. https://doi.org/10.1016/j.ijfatigue.2021.106205.
[5] Mohabeddine A, Correia JAF, Castro J, Montenegro P, De Jesus AM, Calçada RA. Numerical investigation on the fatigue life of non-cracked metallic plates repaired with bonded CFRP. ce/papers Sep. 2021;4(2–4):1135–44. https://doi.org/10.1002/cepa.1405.
[6] Mohabeddine A, et al. Experimental parametric investigation on the behavior of adhesively bonded CFRP/steel joints. Compos Struct Dec. 2022:116598. https://doi.org/10.1016/j.compstruct.2022.116598.
[7] Yu T, Fernando D, Teng JG, Zhao XL. Experimental study on CFRP-to-steel bonded interfaces. Compos Part B Eng 2012;43(5):2279–89. https://doi.org/10.1016/j.compositesb.2012.01.024.
[8] Russian O, Khan S, Belarbi A, Dawood M. Effect of surface preparation technique on bond behavior of CFRP-steel double-lap joints: Experimental and numerical studies. Compos Struct Jan. 2021;255:113048. https://doi.org/10.1016/j.compstruct.2020.113048.
[9] Xia SH, Teng JG. Behavior of FRP to steel bonded joint. In: Procedding of the International Symposium on Bon Behaviour of FRP in Structures (BBFS 2005), Jan. 205AD, pp. 411–418, [Online]. Available: http://espace.library.uq.edu.au/view/UQ:376041.
[10] Fawzia S, Zhao XL, Al-Mahaidi R. Bond-slip models for double strap joints strengthened by CFRP. Compos Struct 2010;92(9):2137–45. https://doi.org/10.1016/j.compstruct.2009.09.042.
[11] Wu C, Zhao X, Duan WH, Al-Mahaidi R. Bond characteristics between ultra high modulus CFRP laminates and steel. Thin-Walled Struct 2012;51:147–57. https://doi.org/10.1016/j.tws.2011.10.010.
[12] Akpinar S. The effect of composite patches on the failure of adhesively-bonded joints under bending moment. Appl Compos Mater 2013;20(6):1289–304. https://doi.org/10.1007/s10443-013-9335-6.
[13] Akpinar S. Effects of laminate carbon/epoxy composite patches on the strength of double-strap adhesive joints: experimental and numerical analysis. Mater Des 2013;51:501–12. https://doi.org/10.1016/j.matdes.2013.04.037.
[14] Ozel A, Yazici B, Akpinar S, Aydin MD, Temiz Ş. A study on the strength of adhesively bonded joints with different adherends. Compos Part B Eng 2014;62:167–74. https://doi.org/10.1016/j.compositesb.2014.03.001.
[15] Fernando D, Teng JG, Yu T, Zhao X. Preparation and Characterization of Steel surfaces for Adhesive Bonding. J Compos Constr 2013;17(6).
[16] Ke L, Li C, Luo N, He J, Jiao Y, Liu Y. Enhanced comprehensive performance of bonding interface between CFRP and steel by a novel film adhesive. Compos Struct 2019;229(June). https://doi.org/10.1016/j.compstruct.2019.111393.
[17] Li C, Ke L, He J, Chen Z, Jiao Y. Effects of mechanical properties of adhesive and CFRP on the bond behavior in CFRP-strengthened steel structures. Compos Struct Mar. 2019;211:163–74. https://doi.org/10.1016/j.compstruct.2018.12.020.
[18] Wang Z, Li C, Sui L, Xian G. Effects of adhesive property and thickness on the bond performance between carbon fiber reinforced polymer laminate and steel. Thin-

Walled Struct 158(September 2020) (2021) 107176, doi: 10.1016/j.tws.2020.107176.
[19] Fawzia S, Al-Mahaidi R, Zhao X. Experimental and finite element analysis of a double strap joint between steel plates and normal modulus CFRP. Compos Struct Sep. 2006;75(1–4):156–62. https://doi.org/10.1016/j.compstruct.2006.04.038.
[20] Jimenez-Vicaria JD, Pulido MDG, Castro-Fresno D. Influence of carbon fibre stiffness and adhesive ductility on CFRP-steel adhesive joints with short bond lengths. Constr Build Mater 2020;260:119758. https://doi.org/10.1016/j.conbuildmat.2020.119758.
[21] Yang Y, Biscaia H, Chastre C, Silva MAG. Bond characteristics of CFRP-to-steel joints. J Constr Steel Res 2017;138:401–19. https://doi.org/10.1016/j.jcsr.2017.08.001.
[22] Pang YY, Wu G, Su ZL, He XY. Experimental study on the carbon-fiber-reinforced polymer–steel interfaces based on carbon-fiber-reinforced polymer delamination failures and hybrid failures. Adv Struct Eng 2020;23(11):2247–60. https://doi.org/10.1177/1369433220911167.
[23] Mohabeddine A, et al. Experimental parametric investigation on the behavior of adhesively bonded CFRP/steel joints (in Press). Compos Struct 2023.
[24] He J, Xian G, Zhang YX. Numerical modelling of bond behaviour between steel and CFRP laminates with a ductile adhesive. Int J Adhes Adhes 2021;104:102753. https://doi.org/10.1016/j.ijadhadh.2020.102753.
[25] SIKA. "PIONEERING STEEL BRIDGE REPAIR: SIKADUR®-370. https://www.sika.com/en/innovation/sika-innovation-flash/pioneering-steel-bridge-repair–sikadur–370.html.
[26] Adams RD, Wake WC. Structural Adhesive Joint in Engineering; 1986.
[27] Hildebrand M. The strength of adhesive-bonded joints between fibre-reinforced plastics and metals: Analysis, shape optimization and experiments. VTT Technical Research Centre of Finland. VTT Publications No. 192; 1994.
[28] Haghani R. Analysis of adhesive joints used to bond FRP laminates to steel members – a numerical and experimental study. Constr Build Mater 2010;24(11):2243–51. https://doi.org/10.1016/j.conbuildmat.2010.04.032.
[29] Doru MO, Özel A, Akpinar S, Aydin MD. Effect of the spew fillet on adhesively bonded single-lap joint subjected to tensile loading: experimental and 3-D non-linear stress analysis. J Adhes 2014;90(3):195–209. https://doi.org/10.1080/00218464.2013.777900.
[30] Akpinar S, Doru MO, Özel A, Aydin MD, Jahanpasand HG. The effect of the spew fillet on an adhesively bonded single-lap joint subjected to bending moment. Compos Part B Eng 2013;55:55–64. https://doi.org/10.1016/j.compositesb.2013.05.056.
[31] Hacısalihoglu İ, Akpinar S. The effect of stepped notches and recesses on joint strength in adhesive bonded joints: experimental and numerical analysis. Theor Appl Fract 119(April, 2022), doi: 10.1016/j.tafmec.2022.103364.
[32] Delzendehrooy F, Ayatollahi MR, Akhavan-Safar A, da Silva LFM. Strength improvement of adhesively bonded single lap joints with date palm fibers: effect of type, size, treatment method and density of fibers. Compos Part B Eng May 2020;188:107874. https://doi.org/10.1016/j.compositesb.2020.107874.
[33] Razavi SMJ, Scott Bale E, Berto F. Mechanical behavior of metallic fiber-reinforced adhesive under cyclic loading. Procedia Struct Integrity 2020;26:225–228. doi: 10.1016/j.prostr.2020.06.026.
[34] Ramezani F, Ayatollahi MR, Akhavan-Safar A, da Silva LFM. A comprehensive experimental study on bi-adhesive single lap joints using DIC technique. Int J Adhes Adhes Oct. 2020;102:102674. https://doi.org/10.1016/j.ijadhadh.2020.102674.
[35] Hart-Smith L. Technical Report NASA-CR-112235. National Aeronautics and Space Administration: Adhesive-bonded double-lap joints. Virgina; 1973.
[36] Akpinar S, Aydin MD, Özel A. A study on 3-D stress distributions in the bi-adhesively bonded T-joints. Appl Math Model 2013;37(24):10220–30. https://doi.org/10.1016/j.apm.2013.06.008.
[37] Öz Ö, Özer H. An experimental investigation on the failure loads of the mono and bi-adhesive joints. J Adhes Sci Technol 2017;31(19–20):2251–70. https://doi.org/10.1080/01694243.2016.1264661.
[38] Marques EAS, Da Silva LFM, Flaviani M. Testing and simulation of mixed adhesive joints for aerospace applications. Compos Part B Eng 2015;74:123–30. https://doi.org/10.1016/j.compositesb.2015.01.005.
[39] da Silva LFM, Lopes MJCQ. Joint strength optimization by the mixed-adhesive technique. Int J Adhes Adhes 2009;29(5):509–14. https://doi.org/10.1016/j.ijadhadh.2008.09.009.
[40] Fitton MD, Broughton JG. Variable modulus adhesives: an approach to optimised joint performance. Int J Adhes Adhes Aug. 2005;25(4):329–36. https://doi.org/10.1016/j.ijadhadh.2004.08.002.
[41] SIKA. Sikadur 30 datasheet. https://zaf.sika.com/content/dam/dms/za01/m/sikadur_-30.pdf.
[42] S&P Reinforcements. S&P HP220 datasheet. https://www.sp-reinforcement.eu/sites/default/files/field_product_col_doc_file/r_resin220hp_pub_tds_prod_resin_220_hp_eu_en_v082020.pdf.
[43] Hautsman advanced materials. Datasheet AW4858/HW4858. [Online]. Available: https://samaro.fr/pdf/FT/Araldite_FT_AW4858_hardener_HW4858_EN.pdf.
[44] ASTM-D638-14. Standard Test Method for Tensile Properties of Plastics. ASTM Stand., 2014;08:1–15.
[45] S&P Reinforcements. Technical datasheet C laminates. [Online]. Available: https://www.sp-reinforcement.eu/sites/default/files/field_product_col_doc_file/r_c-laminates_pub_tds_prod_c-laminates_v4.102020_eu_en.pdf.
[46] Clarke JL. EUROCOMP: Structural Design of Polymer composites. London: Chapman & Hall; 1996.
[47] da Silva LF, Pirondi A, Ochsner A. Hybrid Adhesive Joints, vol. 6. Berlin, Heidelberg: Springer, Berlin Heidelberg; 2011.
[48] Pires I, Quintino L, Durodola JF, Beevers A. Performance of bi-adhesive bonded aluminium lap joints. Int J Adhes Adhes 2003;23(3):215–23. https://doi.org/10.1016/S0143-7496(03)00024-1.
[49] Majidi HR, Razavi SMJ, Berto F. Failure assessment of steel/CFRP double strap joints. Metals (Basel) 2017;7(7):1–16. https://doi.org/10.3390/met7070255.
[50] Zhao XL, Zhang L. State-of-the-art review on FRP strengthened steel structures. Eng Struct 2007;29(8):1808–23. https://doi.org/10.1016/j.engstruct.2006.10.006.
[51] Li C, Ke L, He J, Chen Z, Jiao Y. Effects of mechanical properties of adhesive and CFRP on the bond behavior in CFRP-strengthened steel structures. Compos Struct 2019;211(December).
[52] Pang Y, Wu G, Wang H, Gao D, Zhang P. Experimental study on the bond behavior of the CFRP-steel interface under rapid loading. Thin-Walled Struct 2021;159(October).
[53] Yang Y, Silva MAG, Biscaia H, Chastre C. CFRP-to-steel bonded joints subjected to cyclic loading: An experimental study. Compos Part B Eng 2018;146(March):28–41. https://doi.org/10.1016/j.compositesb.2018.03.039.
[54] Wang TT, Ryan FW, Schonhorn H. Effect of bonding defects on shear strength in tension of lap joints having brittle adhesives. J Appl Polym Sci Aug. 1972;16(8):1901–9. https://doi.org/10.1002/app.1972.070160804.
[55] Marques EAS, da Silva LFM. Joint strength optimization of adhesively bonded patches. J Adhes 2008;84(11):915–34. https://doi.org/10.1080/00218460802505275.
[56] Al-zubaidy H, Al-mahaidi R, Zhao X. Finite element modelling of CFRP / steel double strap joints subjected to dynamic tensile loadings. Compos Struct 2013;99:48–61. https://doi.org/10.1016/j.compstruct.2012.12.003.
[57] Al-mosawe A, Al-mahaidi R, Zhao X. Bond behaviour between CFRP laminates and steel members under different loading rates. Compos Struct 2016;148:236–51. https://doi.org/10.1016/j.compstruct.2016.04.002.
[58] Li H, Xu S, Zhang Z, Song C. Experimental and numerical investigation on the corrosion effects on the bonding behavior between CFRP and steel. Compos Struct 2021;259(December).
[59] Yang Y, Zhao J, Zhang S, Chastre C, Biscaia H. Effect of mechanical anchorage on the bond performance of double overlapped CFRP-to-steel joints. Compos Struct 2021;267(November).
[60] Haghani R. Finite element modelling of adhesive bonds joining fibre-reinforced polymer (FRP) composites to steel. In: Rehabilitation of Metallic Civil Infrastructure Using Fiber Reinforced Polymer (FRP) Composites, Chalmers U., Sweden: Elsevier; 2014. p. 60–95.
[61] Xin H, Mosallam A, Liu Y, Wang C, Zhang Y. Analytical and experimental evaluation of flexural behavior of FRP pultruded composite profiles for bridge deck structural design. Constr Build Mater 2017;150:123–49. https://doi.org/10.1016/j.conbuildmat.2017.05.212.
[62] Xin H, Liu Y, Mosallam AS, He J, Du A. Evaluation on material behaviors of pultruded glass fiber reinforced polymer (GFRP) laminates. Compos Struct 2017;182:283–300. https://doi.org/10.1016/j.compstruct.2017.09.006.
[63] SImpson-Strong-Tie. Safety data sheet: S&P C-Laminate SM (150/2000) & S&P C-Laminate HM (200/2000). 2022. [Online]. Available: https://strongtie.com.au/sites/default/files/msds/SDS-CLAMINATE-NA-ENG-0822.pdf.
[64] Wypych G. VE vinyl ester resin. In: Handbook of Polymers, Second Edi., G. Wypych, Ed. Elsevier; 2016. p. 702–703.
[65] Krucinska I, Stypka T. Direct measurement of the axial poisson's ratio of single carbon fibres. Compos Sci Technol 1991;41(1):1–12. https://doi.org/10.1016/0266-3538(91)90049-U.
[66] Christensen RM. Properties of carbon fibers. J Mech Phys Solids 1994;42(4):681–95. https://doi.org/10.1016/0022-5096(94)90058-2.
[67] Kumar S. Advanced Materials: Challenge Next Decade. In: Proc Znt SAMPE Symp Exhib 35;1990:2224–2235.
[68] Miyagawa H, Sato C, Mase T, Drown E, Drzal LT, Ikegami K. Transverse elastic modulus of carbon fibers measured by Raman spectroscopy. Mater Sci Eng A 2005;412(1–2):88–92. https://doi.org/10.1016/j.msea.2005.08.037.
[69] Akpinar S, Demir K, Gavgali E, Yetim AF. A study on the effects of nanostructure reinforcement on the failure load in adhesively bonded joints after the subjected to fully reversed fatigue load. J Adhes 2022;98(13):1972–97. https://doi.org/10.1080/00218464.2021.1947811.
[70] Mohabeddine A, Eshaghi C, Correia JAFO, Castro JM. Analytical investigation of the cyclic behaviour of I-shaped steel beam with reinforced web using bonded CFRP. J. Steel Compos Struct 2022.